Journal of Computational Physics **164,** 104–122 (2000)
doi:10.1006/jcph.2000.6586, available online at http://www.idealibrary.com on IDEAL®

A Flux-Splitting Scheme for Compressible and Incompressible Flows

Cord-Christian Rossow

DLR, Deutsches Zentrum für Luft- und Raumfahrt, Institut für Entwurfsaerodynamik, 38022 Braunschweig, Germany
E-mail: cord.rossow@dlr.de

Received August 16, 1999; revised March 12, 2000

In the present work, a recently proposed flux-splitting scheme suitable for compressible flow is extended to incompressible flows. Appropriate dissipation terms for both incompressible and compressible flows are determined by expanding the Roe flux-difference splitting in terms of Mach number. Analysis of the dissipation terms in this form for both the Roe scheme and the basic (current) scheme leads to the incorporation of certain terms into the basic scheme to establish the transition from compressible flow toward the incompressible limit. Using the proper terms in the dissipation formulation, convergence rates for airfoil flows became nearly independent of the freestream Mach number. © 2000 Academic Press

Key Words: flux-splitting scheme; compressible and incompressible flows; relevant terms for all speeds; Navier–Stokes.

1. INTRODUCTION

The requirements for discretization methods suitable for the simulation of technically relevant flows cover a very broad spectrum, and are sometimes even contradicting: To obtain accurate solutions, only a minimum amount of numerical viscosity can be tolerated, especially for the resolution of boundary layers in viscous flows. For flows with strong shock waves, however, robustness becomes of primary importance, especially near vacuum conditions where the prediction of negative values for positive quantities like pressure and density is likely to occur. In such situations, the proper amount of numerical viscosity needs to be supplied to achieve a converged solution. To establish adequate discretization schemes, recent development has focused on construction of hybrid flux-splitting formulations, where the accuracy of flux-difference splitting [1] is combined with the robustness of flux-vector splitting [2]. Prominent representatives of such schemes are the advection upstream split Mach number (AUSM) scheme [3], the low-diffusion flux-splitting scheme (LDFSS) [4], and the convection upstream split pressure (CUSP) formulations [5, 6]. In a previous study

0021-9991/00 $35.00

[7], an alternative formulation based on the left and right Mach numbers was proposed. Here, the computation of an intermediate state at a cell interface is almost completely avoided. The derivation in [7] leads to a very simple discretization scheme, which despite its simplicity rivals the common, most advanced high-resolution/high-accuracy schemes such as [3–5].

In addition to the derivation of numerical methods for computation of compressible flows, over the past several years considerable effort has been spent on the extension of schemes designed for compressible flow to solve for incompressible flow. The problems of compressible codes handling incompressible flows are caused by the disparity of the eigenvalues of the compressible equations: at low speeds, the largest eigenvalue tends toward the speed of sound, whereas the smallest eigenvalue approaches zero. Thus, the ratio of largest to smallest eigenvalue, the condition number of the system of equations, tends to infinity and the stiffness of the system of equations increases. To overcome the stiffness problem, the eigenvalues are altered toward a more favorable condition number, and the system of equations is "preconditioned" for easier solution with iterative methods, e.g., [8–10].

In the present work, the requirements of both compressible and incompressible flows for the formulation of the discrete interface flux function are considered. The intention of this work is to establish a discretization method suitable for the range from incompressible to hypersonic flows without overly compromising accuracy or robustness. As a basis, the flux-splitting scheme derived in [7] will be used. The scheme employs elements of the LDFSS [4] and of the CUSP [5] formulations and uses the left and right Mach number at an interface to establish the flux function. The basic scheme is extended to incompressible flows. To identify terms important in the incompressible limit, the Roe flux-difference splitting [1] is expanded in functions of the Mach number. Analysis of the resulting expressions leads to the incorporation of certain terms establishing an appropriate discretization scheme at low speeds. The implications for the convergence characteristics of the extended scheme are then assessed for viscous airfoil flows at incompressible and at transonic conditions.

2. GOVERNING EQUATIONS

We consider the two-dimensional Navier–Stokes equations for compressible flow. The system of partial differential equations in strong conservation form is given by

$$\frac{\partial \mathbf{W}}{\partial t} + \frac{\partial \mathbf{F}}{\partial x} + \frac{\partial \mathbf{G}}{\partial y} = 0, \tag{1}$$

where $\mathbf{W}$ represents the vector of conservative variables. The flux-density vectors for the x and y directions, $\mathbf{F}$ and $\mathbf{G}$, may be split in convective and viscous parts according to

$$\mathbf{F} = \mathbf{F}_c - \mathbf{F}_v; \quad \mathbf{G} = \mathbf{G}_c - \mathbf{G}_v. \tag{2}$$

Setting the viscous parts of the flux-density tensor, $\mathbf{F}_v$ and $\mathbf{G}_v$, to zero, the Euler equations governing inviscid flow are obtained.

In the construction of hybrid flux-splitting upwind schemes, it was recognized that the convective parts of the flux-density vectors may be further subdivided into contributions related to advection and pressure [3, 5]:

$$\mathbf{F}_c = \mathbf{F}_{ad} + \mathbf{F}_p; \quad \mathbf{G}_c = \mathbf{G}_{ad} + \mathbf{G}_p, \tag{3}$$

where the contributions due to pressure are defined as

$$\mathbf{F}_{\mathrm{p}} = \begin{bmatrix} 0 \\ p \\ 0 \\ 0 \end{bmatrix}; \quad \mathbf{G}_{\mathrm{p}} = \begin{bmatrix} 0 \\ 0 \\ p \\ 0 \end{bmatrix}, \tag{4}$$

and the contributions related to advection are given by

$$\mathbf{F}_{\mathrm{ad}} = u\phi; \quad \mathbf{G}_{\mathrm{ad}} = v\phi, \tag{5}$$

with the vector of advected quantities defined by

$$\phi = \begin{bmatrix} \rho \\ \rho u \\ \rho v \\ \rho H \end{bmatrix}. \tag{6}$$

3. HYBRID FLUX-SPLITTING SCHEME FOR COMPRESSIBLE FLOW

In the following, a brief presentation of the hybrid flux-splitting scheme MAPS developed in [7] and an overview of the basic solution method will be given. For the design principles of the MAPS (Mach number-based advection pressure splitting) scheme the reader is referred to [7].

3.1. *Basic Discretization Scheme*

The flux-splitting scheme developed in [7] splits the convective flux-density tensor into an advective contribution and into a contribution associated with pressure, Eq. (3). The advective part $\mathbf{F}^{\phi}$ at a cell interface is discretized by

$$\begin{aligned} \mathbf{F}^{\phi} = {} & \frac{1}{2}\left(q_{\mathrm{n}}^{\mathrm{L}} + q_{\mathrm{n}}^{\mathrm{R}}\right) \cdot \frac{1}{2}\left(\phi_{\mathrm{n}}^{\mathrm{L}} + \phi_{\mathrm{n}}^{\mathrm{R}}\right) - \frac{1}{2}(\phi^{\mathrm{L}} + \phi^{\mathrm{R}}) \cdot \frac{1}{2}\beta^{M} \cdot c^{\mathrm{av}} \cdot [M^{\mathrm{R}} \cdot \mathrm{sign}(M^{\mathrm{R}}) \\ & - M^{\mathrm{L}} \cdot \mathrm{sign}(M^{\mathrm{L}})] - \frac{1}{2} \cdot c^{\mathrm{av}} \cdot \max(|M^{\mathrm{L}}|, |M^{\mathrm{R}}|) \cdot (\phi^{\mathrm{R}} - \phi^{\mathrm{L}}), \end{aligned} \tag{7}$$

where L and R denote the states left and right of the cell interface, q_{n} is the normal velocity at the interface, M denotes the Mach number of the interface normal velocity, evaluated by

$$M = \frac{q_{\mathrm{n}}}{c^{\mathrm{av}}}, \tag{8}$$

and c^{av} is the average speed of sound at the interface computed by

$$c^{\mathrm{av}} = \frac{1}{2}(c^{\mathrm{L}} + c^{\mathrm{R}}). \tag{9}$$

The function β^{M} is given by

$$\begin{aligned} \beta^{\mathrm{M}} &= \max(0, 2 \cdot M^{\max 1} - 1) \\ M^{\max 1} &= \min\lfloor \max(|M^{L}|, |M^{R}|), 1 \rfloor. \end{aligned} \tag{10}$$

The contribution of pressure at a cell interface is determined via

$$\mathbf{F}^{\mathrm{p}} = \frac{1}{2}(\mathbf{p}^{\mathrm{L}} + \mathbf{p}^{\mathrm{R}}) - \frac{1}{2} \cdot \beta^{\mathrm{p}} \cdot [\mathbf{p}^{\mathrm{R}} \cdot \mathrm{sign}(M^{\mathrm{R}}) - \mathbf{p}^{\mathrm{L}} \cdot \mathrm{sign}(M^{\mathrm{L}})], \tag{11}$$

where

$$\mathbf{p} = \begin{bmatrix} 0 \\ p \cdot n_x \\ p \cdot n_y \\ 0 \end{bmatrix}; \quad \mathbf{n} = \begin{bmatrix} n_x \\ n_y \end{bmatrix}, \tag{12}$$

with $\mathbf{n}$ denoting the unit normal vector of the interface, and the blending function β^{p} defined as

$$\begin{aligned} \beta^{\mathrm{p}} &= \max(0, 2 \cdot M^{\min 1} - 1) \\ M^{\min 1} &= \min[\min(|M^{\mathrm{L}}|, |M^{\mathrm{R}}|), 1]. \end{aligned} \tag{13}$$

3.2. *Basic Solution Algorithm*

The basic solution scheme is a cell-centered, finite-volume scheme, where the time integration is performed using a 5-stage Runge–Kutta scheme. The MAPS scheme is implemented in the pattern of a central discretization plus artificial dissipation, and the artificial dissipative terms are evaluated at every odd stage of the time-marching scheme. For second-order accuracy, the components of the advection vector ϕ are reconstructed. To control the reconstruction, the SLIP limiter of [5] is used following the implementation given in [6]. To accelerate convergence toward the steady state, local time-stepping, implicit residual averaging, and Multigrid are used. The influence of turbulence is modeled according to Baldwin and Lomax [11]. The basic outline of the numerical framework may be found in [12].

If not otherwise indicated, in the following computations the numerical parameters are fixed to

CFL = 7.5
4-level W cycle
First-order MAPS scheme on coarse meshes
Modification of SLIP-limiter according to Swanson *et al.* [6] by setting $k^{(4)} = 1/8$.

4. FLUX-SPLITTING SCHEME FOR COMPRESSIBLE AND INCOMPRESSIBLE FLOW

Preconditioning methods have been developed to solve incompressible flow problems with numerical algorithms designed primarily for compressible flows. The difficulties encountered with low-speed flows arise from the increase in the condition number of the system of equations, i.e., the increase in the stiffness of the governing equations. To overcome the stiffness problem, the time derivatives of the dependent variables are multiplied by a suitable matrix in order to change the eigenvalues such that the condition number is more favorable. This may be expressed by

$$\mathbf{P}^{-1} \frac{\Delta \mathbf{W}}{\Delta t} + \frac{\partial \mathbf{F}}{\partial x} + \frac{\partial \mathbf{G}}{\partial y} = AD, \tag{14}$$

where $\mathbf{P}^{-1}$ is the preconditioning matrix, and AD denotes the artificial dissipative terms

necessary to stabilize the numerical scheme. Note that in Eq. (14) the spatial derivatives of the flux-density tensor are assumed to be approximated by central difference approximations. As outlined in [9, 10], for a Roe-type scheme the artificial dissipation should be based on the eigenvalues of the preconditioned Jacobians:

$$\frac{\Delta \mathbf{W}}{\Delta t} + \mathbf{P} \cdot \left[\frac{\partial \mathbf{F}}{\partial x} + \frac{\partial \mathbf{G}}{\partial y} \right] = \mathbf{P}[(|\mathbf{P}^{-1} \cdot \mathbf{A}|\Delta \mathbf{W})_x + (|\mathbf{P}^{-1} \cdot \mathbf{B}|\Delta \mathbf{W})_y], \tag{15}$$

where $\mathbf{A}$ and $\mathbf{B}$ denote the Jacobians of the x and y directions, and $\mathbf{P}^{-1}\mathbf{A}$ and $\mathbf{P}^{-1}\mathbf{B}$ are the corresponding preconditioned Jacobians. In the case of a CUSP scheme, for Mach numbers below 0.5 the artificial dissipation scales linearly with the normal interface velocity. Thus, in [6] the preconditioning was applied in the form

$$\frac{\Delta \mathbf{W}}{\Delta t} + \mathbf{P}\left[\frac{\partial \mathbf{F}}{\partial x} + \frac{\partial \mathbf{G}}{\partial y} - (\mathbf{P}^{-1}|q_{\mathrm{n}}|\Delta \mathbf{W})_n \right] = 0; \tag{16}$$

i.e., the numerical dissipation need not be changed. Since the MAPS and the CUSP scheme yield similar expressions for Mach numbers below 0.5, this strategy was at first adopted for the computation of low-speed flows. In the present study, however, it was found advantageous for MAPS to implement the numerical viscosity in the form

$$\frac{\Delta \mathbf{W}}{\Delta t} + \mathbf{P}\left[\frac{\partial \mathbf{F}}{\partial x} + \frac{\partial \mathbf{G}}{\partial y} \right] = |q_{\mathrm{n}}|\Delta \mathbf{W}; \tag{17}$$

i.e., only the centrally differenced fluxes are preconditioned and the artificial dissipation is added after the preconditioning step. Note that this implementation leads to a nonconservative formulation of the artificial dissipation.

In the present investigation, the preconditioning matrix given by Choi and Merkle [8] is used to remove the stiffness in the system of equations. In all preconditioners developed so far, a reference Mach number M_{r} must be computed in order to avoid numerical difficulties at stagnation points. In the present study the reference Mach number M_{r} is evaluated from

$$M_{\mathrm{r}}^2 = \min\left[\max\left(\frac{q^2}{c^2}, k\frac{q_\infty^2}{c_\infty^2} \right), 1 \right], \tag{18}$$

where q and c denote velocity and speed of sound, respectively. The constant k in (18) is set to $k = 1$, unless otherwise noted.

Figure 1 shows the convergence rates obtained for the computation of the viscous flow around the RAE2822 airfoil for a freestream Mach number of $M_\infty = 0.001$ and $M_\infty = 0.73$. A mesh with C-topology using 320×64 cells was employed. In both cases the preconditioning matrix of [8] was used with the implementation given by Eq. (17). The corresponding slopes are indicated in the figure by $\mathrm{pr} = 2$. As can be seen in Fig. 1, the computation of the incompressible flow poses no severe problem, but the convergence rate of the preconditioned code now deteriorates for compressible flow. This becomes clear by comparison with the unpreconditioned result, the convergence history denoted by $\mathrm{pr} = 0$ in the figure.

Regarding the results in Fig. 1, it becomes obvious that certain elements in the basic MAPS scheme are missing if one attempts to establish a convergence behavior independent of compressible or incompressible conditions. When inspecting hybrid flux-splitting

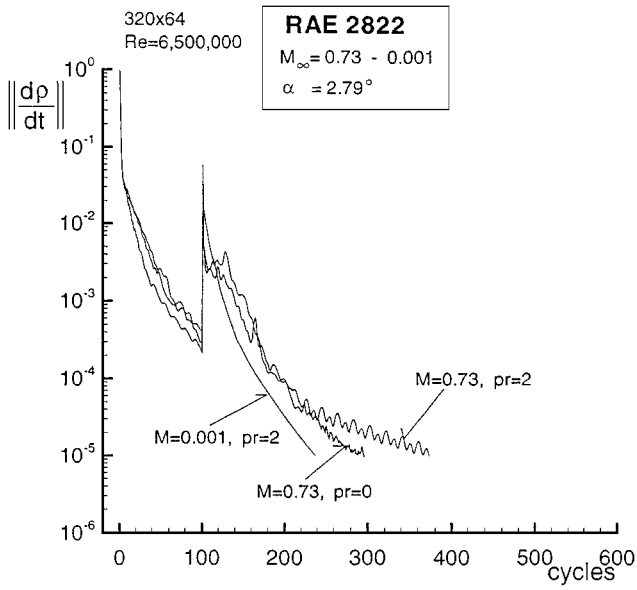

FIG. 1. Basic MAPS scheme and preconditioning.

schemes like AUSM, LDFSS, CUSP, or MAPS, one notices that these schemes do not provide any crossflow diffusion for grid-aligned flows, since for the aligned cell face the normal component of velocity approaches zero. In principle, the schemes are designed that way to accurately resolve shear layers. However, in the Roe flux-difference splitting (FDS), crossflow diffusion is provided by acoustic and shear waves even for an interface normal velocity of zero. Therefore, in the following the Roe FDS scheme will be expanded in terms of Mach number to identify relevant terms when the interface normal velocity approaches zero.

4.1. *Expansion of Roe FDS in Terms of Mach Number and Augmented MAPS Formulation*

The basic Roe flux-differencing scheme is given by

$$\mathbf{F}^{\mathrm{Roe}} = \frac{1}{2}(\mathbf{F}^{\mathrm{L}} + \mathbf{F}^{\mathrm{R}}) - \frac{1}{2}|\mathbf{A}|\Delta\mathbf{W}, \tag{19}$$

where $\mathbf{F}^{\mathrm{L}}$ and $\mathbf{F}^{\mathrm{R}}$ are the left and right states of the inviscid, convective part of the flux-density vector, $\mathbf{A}$ is the corresponding flux Jacobian, and $\Delta\mathbf{W}$ denotes the differences in conservative variables between the left and the right state of the interface. For the expansion, the interface Mach number M_0 is defined as

$$M_0 = \min(|M|, 1) \cdot \mathrm{sign}(M); \tag{20}$$

i.e., M_0 denotes the unaltered interface Mach number, however bounded by ± 1. Using this definition, the expression $|\mathbf{A}|\Delta\mathbf{W}$ in Eq. (19), which represents the dissipative terms of the FDS scheme, is expanded in terms factored by M_0 and $(1 - |M_0|)$. To derive the Mach number expansion, the basic derivation of Roe and Pike [13] was used as a guideline. The resulting expressions are summarized in Eq. (21), Table I. Here ΔF_ρ, $\Delta F_{\rho u}$, $\Delta F_{\rho v}$, $\Delta F_{\rho H}$ denote the expressions of $|\mathbf{A}|\Delta\mathbf{W}$ for the continuity, the momentum, and the energy equation, respectively. All intermediate variables on a cell interface must be evaluated using Roe-averaging [1], as it is standard practice for the matrix $|\mathbf{A}|$ in the classical FDS scheme. Note

TABLE I
Eq. (21): Flux-Difference Dissipation Expanded in Mach Number

$\Delta F_\rho =$	$\frac{1}{c}(1-\lvert M_0\rvert)\Delta p$		$+\rho\lvert M_0\rvert\Delta q_n$	$+\lvert q_n\rvert\Delta\rho$
$\Delta F_{\rho u} = n_x\lvert M_0\rvert\Delta p$	$+\frac{1}{c}u(1-\lvert M_0\rvert)\Delta p$	$+n_x\rho c(1-\lvert M_0\rvert)\Delta q_n$	$+\rho u\lvert M_0\rvert\Delta q_n$	$+\lvert q_n\rvert\Delta\rho u$
$\Delta F_{\rho v} = n_y\lvert M_0\rvert\Delta p$	$+\frac{1}{c}v(1-\lvert M_0\rvert)\Delta p$	$+n_y\rho c(1-\lvert M_0\rvert)\Delta q_n$	$+\rho v\lvert M_0\rvert\Delta q_n$	$+\lvert q_n\rvert\Delta\rho v$
$\Delta F_{\rho H} =$	$\frac{1}{c}H(1-\lvert M_0\rvert)\Delta p$ $-\lvert q_n\rvert(1-\lvert M_0\rvert)\Delta p$	$+q_n\rho c(1-\lvert M_0\rvert)\Delta q_n$	$+\rho H\lvert M_0\rvert\Delta q_n$	$+\lvert q_n\rvert\Delta\rho H$

that the terms given in Eq. (21) must be multiplied by 0.5 to obtain the correct scaling for the dissipative terms of the FDS scheme; see Eq. (19). Proceeding from left to right in Eq. (21), the following terms should be noted:

—In the momentum equations, the upwinding of pressure is achieved by linearly scaling the pressure differences Δp by $|M_0|$.

—In all equations pressure differences are added, scaled by $\frac{1}{c}(1-|M_0|)$. Note that these terms are switched off at supersonic flow.

—In the energy equation, an additional term with pressure differences occurs. This term arises from the fact that differences $\Delta\rho H$ are used for the dissipative flux instead of $\Delta\rho E$. Note that this term vanishes at $|M|=1$ and $M=0$.

—With the exception of the continuity equation, in all other equations differences in the normal velocity Δq_n scaled by $\rho c(1-|M_0|)$ appear. These terms vanish for supersonic flow, and in the energy equation the term also vanishes for $M\to 0$.

—In all equations differences in normal velocity Δq_n occur, scaled linearly by $|M_0|$. These terms provide the upwinding of the normal interface velocity.

—In all equations, differences in the advected quantities $\Delta\phi$ are scaled linearly by the normal velocity at an interface.

To identify terms in the Roe scheme that contribute to crossflow diffusion, let the interface normal velocity q_n and, correspondingly, M_0 approach zero. The remaining terms are summarized in Eq. (22), Table II.

It is instructive to compare the corresponding formulations of the MAPS scheme with the expressions in Eq. (21), Table I. The formulations for the MAPS scheme are given in Eq. (23), Table III, where corresponding terms are located at the same positions as in Table I. Comparison of Table I with Table III reveals that construction of the MAPS scheme bears a

TABLE II
Eq. (22): Crossflow Diffusion of Roe Scheme

$\Delta F_\rho^{\text{cross}} =$	$\frac{1}{c}(1-\lvert M_0\rvert)\Delta p$	
$\Delta F_{\rho u}^{\text{cross}} =$	$\frac{1}{c}u(1-\lvert M_0\rvert)\Delta p$	$+n_x\rho c(1-\lvert M_0\rvert)\Delta q_n$
$\Delta F_{\rho v}^{\text{cross}} =$	$\frac{1}{c}v(1-\lvert M_0\rvert)\Delta p$	$+n_y\rho c(1-\lvert M_0\rvert)\Delta q_n$
$\Delta F_{\rho H}^{\text{cross}} =$	$\frac{1}{c}H(1-\lvert M_0\rvert)\Delta p$	

TABLE III
Eq. (23): MAPS Dissipation

$\Delta F_\rho =$	$+\rho\beta^{\mathrm{M}}\Delta q_{\mathrm{n}}$	$+\lvert q_{\mathrm{n}}\rvert\Delta\rho$
$\Delta F_{\rho u} = n_x\beta^{\mathrm{p}}\Delta p$	$+\rho u\beta^{\mathrm{M}}\Delta q_{\mathrm{n}}$	$+\lvert q_{\mathrm{n}}\rvert\Delta\rho u$
$\Delta F_{\rho v} = n_y\beta^{\mathrm{p}}\Delta p$	$+\rho v\beta^{\mathrm{M}}\Delta q_{\mathrm{n}}$	$+\lvert q_{\mathrm{n}}\rvert\Delta\rho v$
$\Delta F_{\rho H} =$	$+\rho H\beta^{\mathrm{M}}\Delta q_{\mathrm{n}}$	$+\lvert q_{\mathrm{n}}\rvert\Delta\rho H$

significant resemblance to the classical Roe scheme. However, all terms scaled by $(1 - |M_0|)$ are omitted, and the scaling for the upwinding of pressure and normal velocity is not performed linearly, but using the functions β^{p} and β^{M} given in Eqs. (13) and (10), respectively. Thus, apart from the terms scaled by $(1 - |M_0|)$, the main difference between the Roe and the MAPS scheme stems from the activation of the upwinding by the functions β^{p} and β^{M}.

As mentioned earlier, when preconditioning is applied to the solution of low-Mach-number flow, the eigenvalues of the preconditioned Jacobian must be used. The matrix of the eigenvalues $\mathbf{\Lambda}^{\mathrm{Pr}}$ of the preconditioned Jacobian $|\mathbf{P}^{-1}\cdot\mathbf{A}_{\mathrm{n}}|$ for the normal direction are given by [9, 10]

$$\mathbf{\Lambda}^{\mathrm{Pr}} = \mathrm{diag}\{q_{\mathrm{n}}, q_{\mathrm{n}}, q'_{\mathrm{n}} + c', q'_{\mathrm{n}} - c'\}, \tag{24}$$

where

$$\begin{aligned} q'_{\mathrm{n}} &= q_{\mathrm{n}}\cdot(1-\alpha),\\ c' &= \sqrt{\alpha^2 q_{\mathrm{n}}^2 + M_{\mathrm{r}}^2 c^2},\\ \alpha &= \frac{1}{2}\left(1 - M_{\mathrm{r}}^2\right), \end{aligned} \tag{25}$$

and M_{r} is given by Eq. (18).

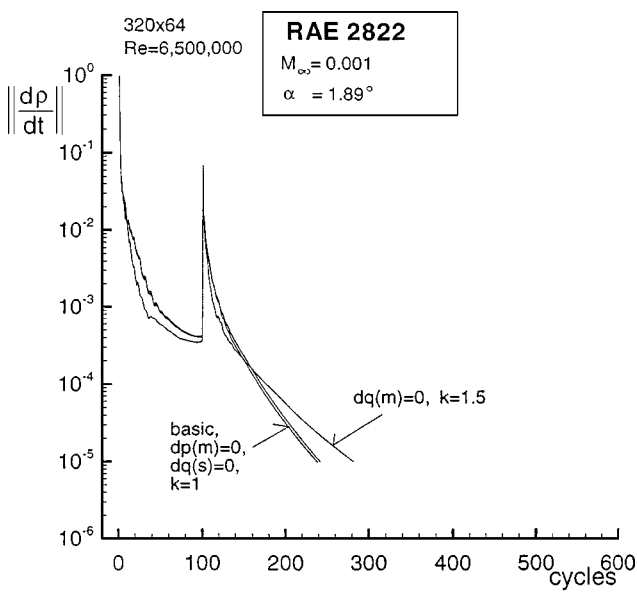

FIG. 2. Flux-difference splitting scheme and preconditioning.

TABLE IV
Eq. (28): Dissipative Terms of MAPS+ Scheme

$\Delta F_\rho =$	$\frac{1}{c}(1-\lvert M_0\rvert)\Delta p$		$+\rho\beta^{\mathrm{M}}\Delta q_{\mathrm{n}}$	$+\lvert q_{\mathrm{n}}\rvert\Delta\rho$
$\Delta F_{\rho u} = n_x\beta^{\mathrm{p}}\Delta p$	$+\frac{1}{c}u(1-\lvert M_0\rvert)\Delta p$	$+n_x\rho c(1-\lvert M_0\rvert)\Delta q_{\mathrm{n}}$	$+\rho u\beta^{\mathrm{M}}\Delta q_{\mathrm{n}}$	$+\lvert q_{\mathrm{n}}\rvert\Delta\rho u$
$\Delta F_{\rho y} = n_y\beta^{\mathrm{p}}\Delta p$	$+\frac{1}{c}v(1-\lvert M_0\rvert)\Delta p$	$+n_y\rho c(1-\lvert M_0\rvert)\Delta q_{\mathrm{n}}$	$+\rho v\beta^{\mathrm{M}}\Delta q_{\mathrm{n}}$	$+\lvert q_{\mathrm{n}}\rvert\Delta\rho v$
$\Delta F_{\rho H} =$	$\frac{1}{c}H(1-\lvert M_0\rvert)\Delta p$		$+\rho H\beta^{\mathrm{M}}\Delta q_{\mathrm{n}}$	$+\lvert q_{\mathrm{n}}\rvert\Delta\rho H$

Approximately, the artificial dissipative terms for the preconditioned Roe scheme are obtained by substituting the preconditioned speed of sound c' from Eq. (25) for the physical speed of sound c in Eq. (21) in Table I and by evaluating M_0 as

$$M_0 = \frac{q'}{c'}. \tag{26}$$

The resulting expressions for the artificial dissipation then resemble closely those in [9]. Following Eq. (16) the preconditioning is now applied as

$$\frac{\Delta \mathbf{W}}{\Delta t} + \mathbf{P}\left[\frac{\partial \mathbf{F}}{\partial x} + \frac{\partial \mathbf{G}}{\partial y} - \mathrm{AD}(q', c')\right] = 0, \tag{27}$$

where AD (q', c') denotes the artificial dissipation terms of the Roe scheme given by Eq. (21), evaluated using the preconditioned variables defined by Eq. (25).

TABLE V
Eq. (29): Evaluation of Interface Variables for MAPS+ Scheme

$\Delta F_\rho =$		$\frac{1}{c^{\max}}(1-\lvert M_0\rvert)\Delta p$		$+\rho\beta^{\mathrm{M}}\Delta q_{\mathrm{n}}$	$+\lvert q_{\mathrm{n}}\rvert\Delta\rho$
$\Delta F_{\rho u} =$	$n_x\beta^{\mathrm{p}}\Delta p$	$+\frac{1}{c^{\max}}u(1-\lvert M_0\rvert)\Delta p$	$+n_x\rho^{\min}c^{\min}(1-\lvert M_0\rvert)\Delta q_{\mathrm{n}}$	$+\rho u\beta^{\mathrm{M}}\Delta q_{\mathrm{n}}$	$+\lvert q_{\mathrm{n}}\rvert\Delta\rho u$
$\Delta F_{\rho y} =$	$n_y\beta^{\mathrm{p}}\Delta p$	$+\frac{1}{c^{\max}}v(1-\lvert M_0\rvert)\Delta p$	$+n_y\rho^{\min}c^{\min}(1-\lvert M_0\rvert)\Delta q_{\mathrm{n}}$	$+\rho v\beta^{\mathrm{M}}\Delta q_{\mathrm{n}}$	$+\lvert q_{\mathrm{n}}\rvert\Delta\rho v$
$\Delta F_{\rho H} =$		$\frac{1}{c^{\max}}H^{\min}(1-\lvert M_0\rvert)\Delta p$		$+\rho H\beta^{\mathrm{M}}\Delta q_{\mathrm{n}}$	$+\lvert q_{\mathrm{n}}\rvert\Delta\rho\mathrm{H}$

$\lvert M_0\rvert = \min(\max(\lvert M^{\mathrm{L}}\rvert, \lvert M^{\mathrm{R}}\rvert), 1)$
$c^{\max} = \max(c^{\mathrm{L}}, c^{\mathrm{R}})$
$c^{\min} = \min(c^{\mathrm{L}}, c^{\mathrm{R}})$
$\rho^{\min} = \min(\rho^{\mathrm{L}}, \rho^{\mathrm{R}})$
$H^{\min} = \min(H^{\mathrm{L}}, H^{\mathrm{R}})$
$u = 0.5 \cdot (u^{\mathrm{L}} + u^{\mathrm{R}})$
$v = 0.5 \cdot (v^{\mathrm{L}} + v^{\mathrm{R}})$
$\rho = 0.5 \cdot (\rho^{\mathrm{L}} + \rho^{\mathrm{R}})$
$\rho u = 0.5 \cdot (\rho^{\mathrm{L}} u^{\mathrm{L}} + \rho^{\mathrm{R}} u^{\mathrm{R}})$
$\rho v = 0.5 \cdot (\rho^{\mathrm{L}} v^{\mathrm{L}} + \rho^{\mathrm{R}} v^{\mathrm{R}})$
$\rho H = 0.5 \cdot (\rho^{\mathrm{L}} H^{\mathrm{L}} + \rho^{\mathrm{R}} H^{\mathrm{R}})$
$\lvert q_{\mathrm{n}}\rvert \rightarrow$ Eq. (7)
$\beta^{\mathrm{M}} \rightarrow$ Eq. (10)
$\beta^{\mathrm{p}} \rightarrow$ Eq. (13)

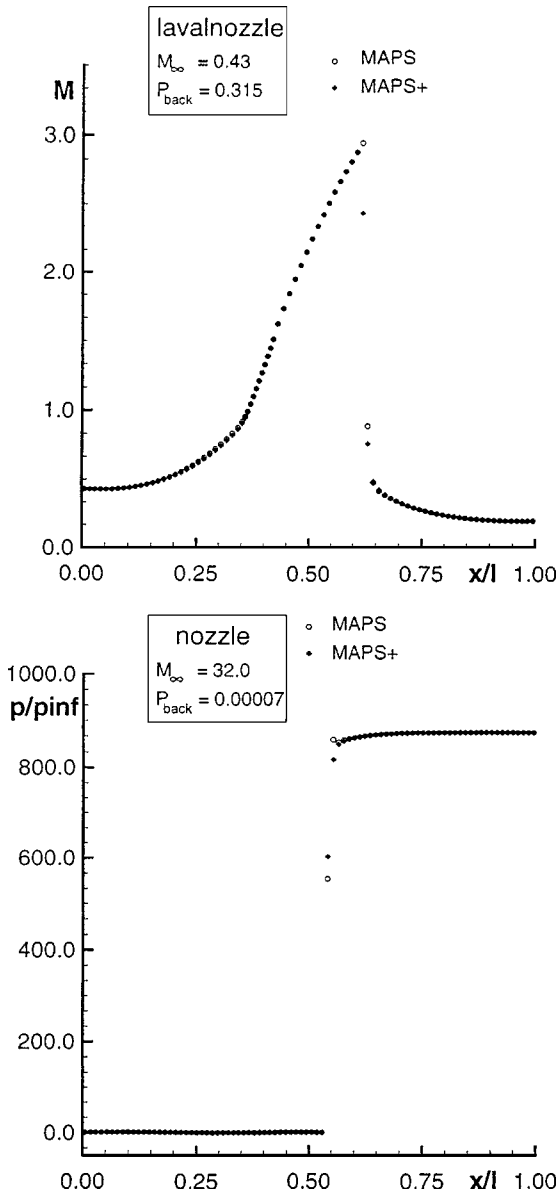

FIG. 3. MAPS and MAPS+ for 1D nozzle flows.

Using the preconditioned Roe scheme, relevant terms in Eq. (21) will now be identified for low Mach number flow. Figure 2 shows the convergence rates for the computation of viscous flow around the RAE2822 at $M_\infty = 0.001, \alpha = 1.89^\circ$, Re = 6,500,000. Two sets of curves can be distinguished in the figure: several almost identical curves showing a fast convergence, and one curve showing a slower convergence. The fast convergence rates were obtained with the basic, preconditioned Roe scheme of Eqs. (21) and (25), and then successively removing the upwind pressure terms of the momentum equations ($dp(m) = 0$), and all normal velocity upwinding terms ($dq(s) = 0$) except the terms $\rho c(1 - |M_0|)\Delta q_n$ in the momentum equations. None of these terms had any significant influence on convergence. Note that the pressure differences scaled by $\frac{1}{c}(1 - |M_0|)$ and the dissipative

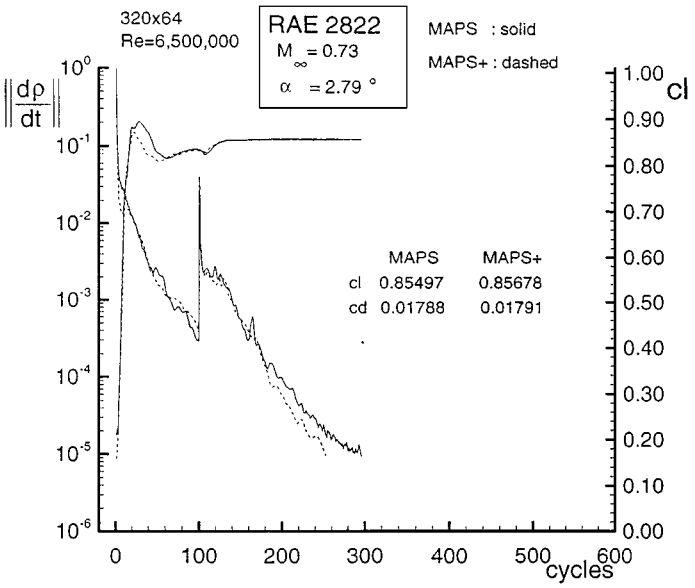

FIG. 4. Comparision for 2D viscous transonic flow.

terms $|q_n|\Delta\phi$ were always retained. However, removing the terms containing the normal velocity upwinding $\rho c(1-|M_0|)\Delta q_n$ in the momentum equations deteriorated the convergence of the scheme considerably ($dq(m)=0$). To establish convergence, the constant k in Eq. (18) had to be increased to 1.5. Thus, numerical experimenting showed that for the

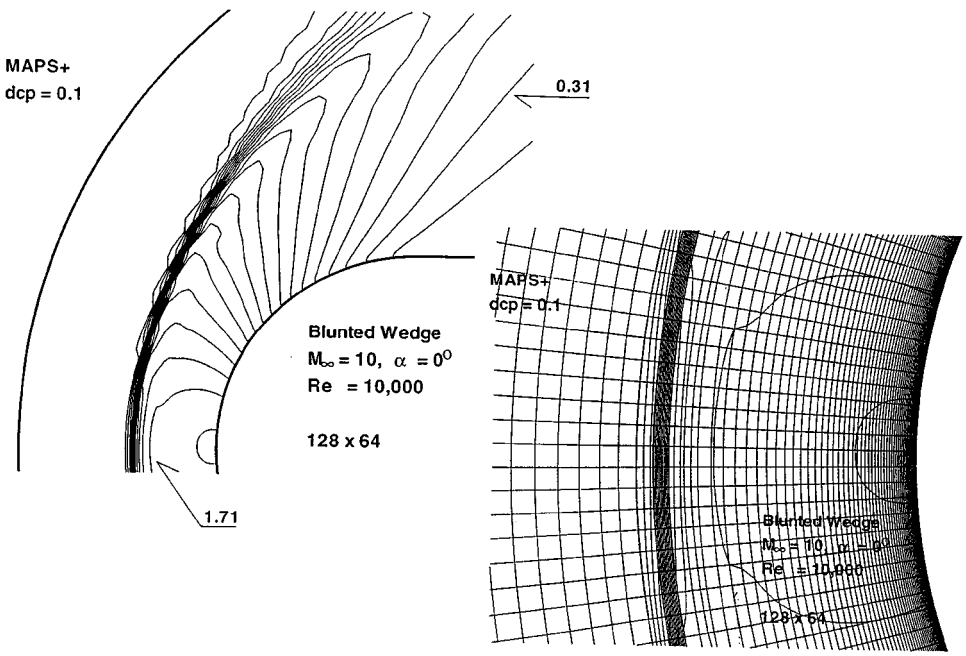

FIG. 5. Results for 2D viscous hypersonic flow with MAPS+ scheme.

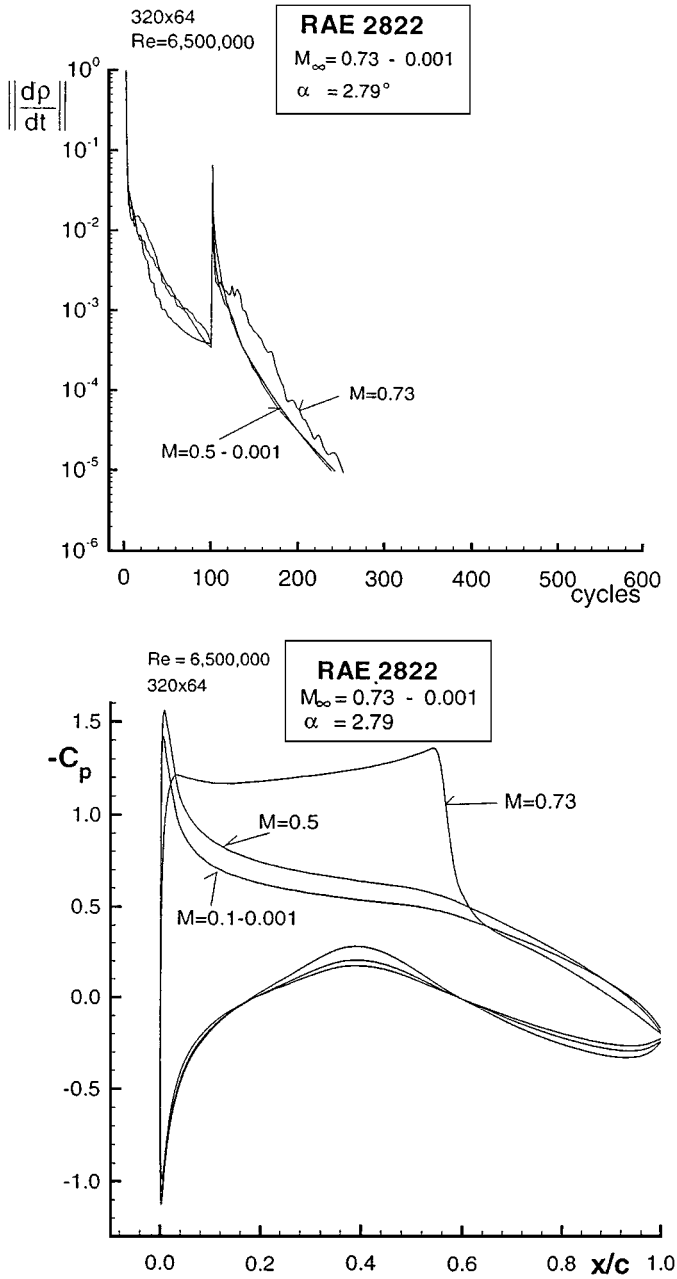

FIG. 6. Mach number variation with preconditioned MAPS+, convergence rates, and pressure distributions.

preconditioned scheme, the important terms are exactly those that provide crossflow diffusion, as summarized in Table II, Eq. (22).

Based on these results, for an augmented MAPS discretization the crossflow diffusion terms of Table II are included in the basic scheme of Table III. The terms of the MAPS+ scheme with crossflow diffusion are listed in Table IV, Eq. (28). To adapt the dissipative terms of MAPS+ given in Table IV for preconditioning, the physical speed of sound in Eq. (28), Table IV, is replaced by the preconditioned speed of sound *c*'. Preconditioning is

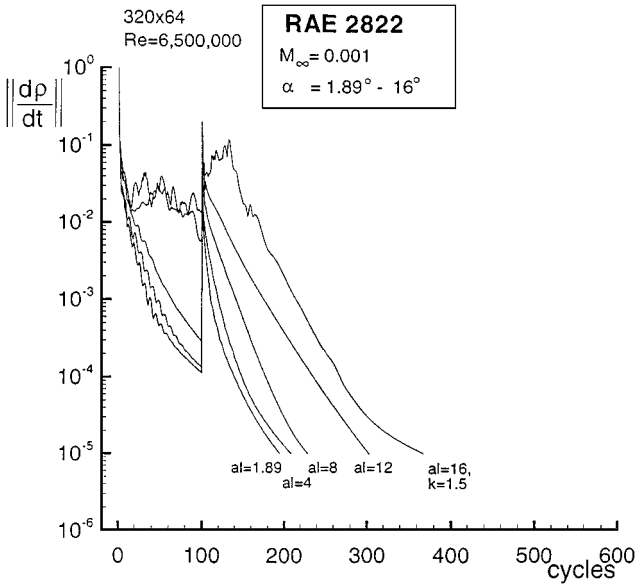

FIG. 7. Variation of angle of attack, convergence rates.

then applied according to Eq. (27) by multiplying the numerical fluxes with the preconditioning matrix **P**. Note that for incorporation in the numerical scheme, the expressions of Table IV must be premultiplied by 0.5 and then subtracted from the centrally discretized flux of the cell interface, as given in Eq. (19) for the FDS scheme. It should be mentioned that the significance of pressure difference terms in preconditioned numerical dissipation was already recognized in [14].

Incorporation of the crossflow diffusion terms to yield the MAPS+ discretization leads to the question of how to evaluate the interface variables needed for the scaling of the pressure and velocity differences. For the FDS scheme, this is done using Roe-averaging. The basic MAPS scheme already possesses very good shock capturing capabilities. Therefore, the influence of the crossflow diffusion terms given in Eq. (22) should be minimized at shocks. This may be established using the procedure given in Table V, Eq. (29). Thus, no Roe-averaging is required for MAPS+.

4.2. *Validation of MAPS+ for Compressible Flow*

Before the computation of incompressible flow with MAPS+ could be started, a check of the performance for the compressible test cases used to validate the basic MAPS scheme in [7] had to be made.

Computation of 1D flow in a Laval nozzle yielded basically the same results as for the basic MAPS scheme, as shown in the upper part of Fig. 3: similarly to MAPS, MAPS+ does not need any entropy condition at sonic points. Also, for strong normal shocks no deterioration compared to MAPS was observed, as can be seen from the computation of 1D nozzle flow with a pre-shock Mach number of 34; see the lower part of Fig. 3. Computation of inviscid 2D flows around airfoils (not shown here) also exhibited no significant differences from the results of the basic MAPS formulation in [7]. A comparison of MAPS and MAPS+ for the viscous flow around the RAE2822 airfoil for the Case 9 conditions of [15],

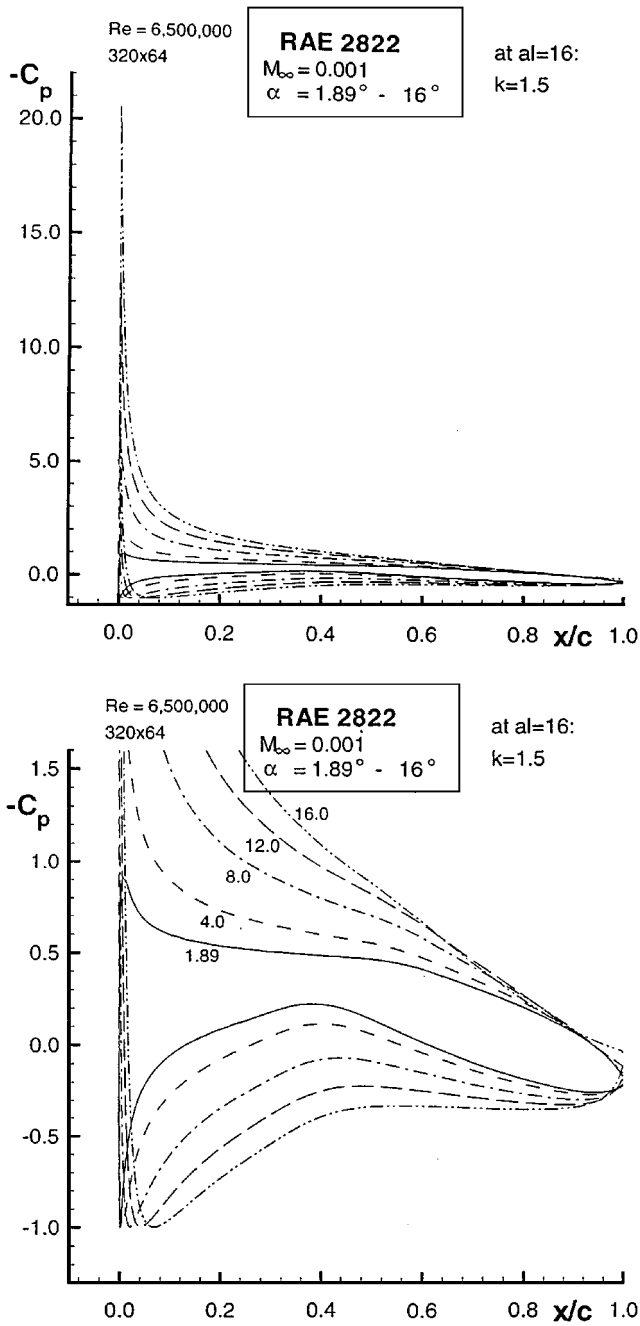

FIG. 8. Variation of angle of attack, pressure distributions.

$M_\infty = 0.73, \alpha = 2.79^\circ$, Re = 6,500,000, is given in Fig. 4. The convergence on the fine mesh has improved using the MAPS+ discretization by about 25% of the fine mesh MG cycles. The computed values for lift and drag are also given in Fig. 4, and as can be seen, the difference is negligible.

The last compressible test case is the hypersonic flow around a blunt body (Fig. 5). Note that for these computations the node-centered code of [6] was used, where the HCUSP

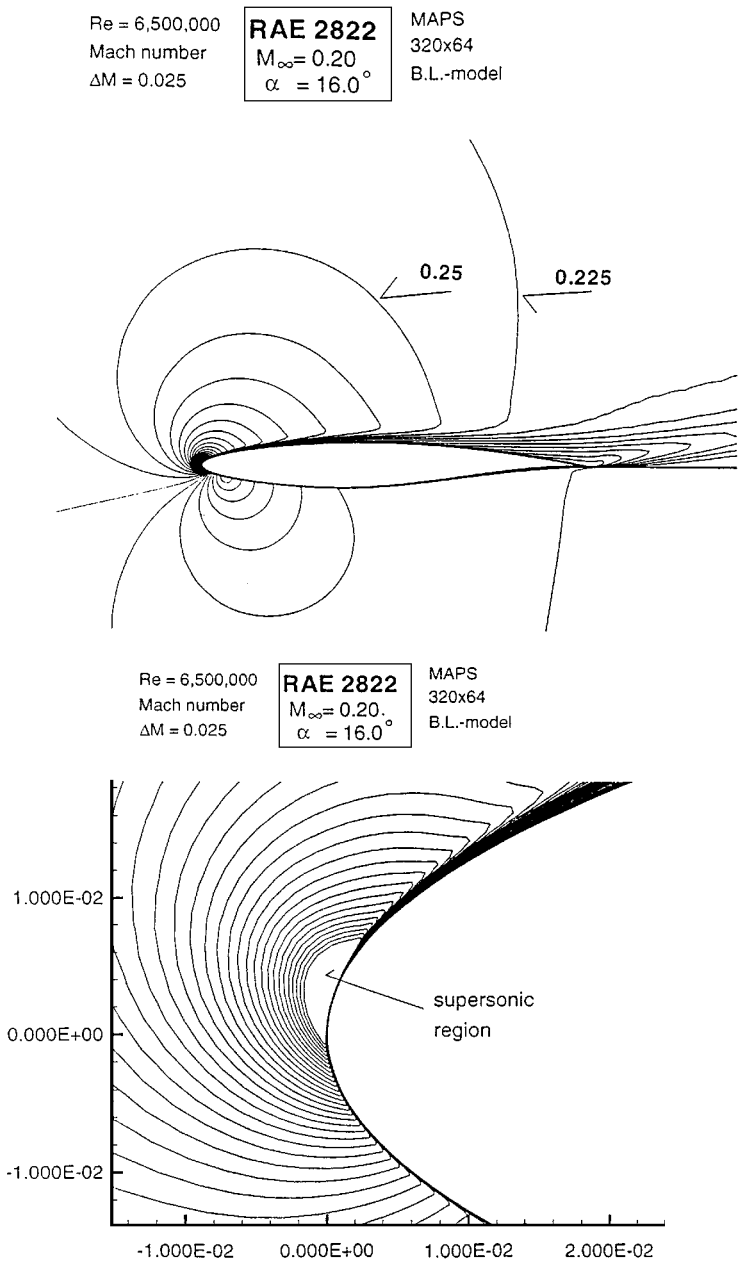

FIG. 9. Mach number distribution for high-lift airfoil flow.

discretization was exchanged for MAPS+. An analogous procedure was used in [7]. The results obtained with MAPS+ are similar to those in [7]. Thus, it is concluded that accuracy and robustness are not impaired by using MAPS+ instead of MAPS for compressible flows.

4.3. *Results for Preconditioned MAPS+ Scheme*

First, the viscous flow around the RAE2822 airfoil is considered. The starting free-stream conditions correspond to Case 9, i.e., $M_\infty = 0.73$, $\alpha = 2.79°$, Re = 6,500,000, and

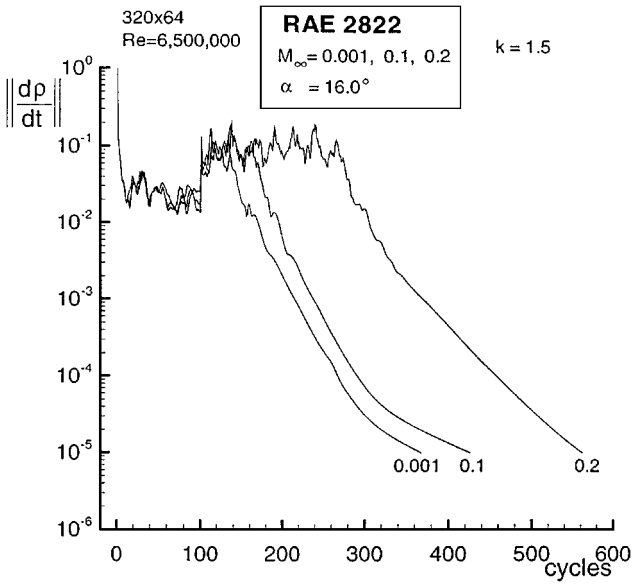

FIG. 10. Convergence rates for high-lift airfoil flow.

transition on upper and lower surface at 3% chord. Keeping all other parameters constant, the Mach number is lowered to $M_\infty = 0.5, 0.1, 0.01, 0.001$, respectively. The change in the pressure distributions due to compressibility effects are clearly seen in Fig. 6; however, the convergence rates are not effected by the variation of Mach number.

In the next step of the investigation, the robustness of the code for computing incompressible flow around airfoils is assessed by a variation of angle of attack at $M_\infty = 0.001$. The Reynolds number is Re = 6,500,000, and the flow is assumed to be fully turbulent to avoid premature separation. As can be seen in Fig. 7, for $\alpha = 1.89°$–$8.0°$, the convergence rates are only slightly affected. For $\alpha = 12°$, convergence problems on the coarse mesh occur; however, a reasonable fine mesh convergence was achieved. At $\alpha = 16°$, a converged solution could be obtained only by increasing the constant k in Eq. (18) to 1.5. Note that after a number of iterations at a high residual level, the convergence rate is close to the other cases. Figure 8 displays computed pressure distributions. At the highest angle of attack, a suction peak of cp = −20.5 is reached. Inspecting the pressure distributions at the trailing edge, it is noted that for the higher angles of attack, $\alpha = 12°$–$16°$, separation at the trailing edge starts, indicated by the smaller amount of pressure recovery. It is assumed that these cases close to separation need more time to settle; once this is established, the asymptotic convergence is similar to the cases without separation. Note that all cases were started from freestream conditions; in none of the cases was the solution of the lower angle of attack used as a starting solution.

The last test case was selected to investigate the convergence properties of the preconditioned MAPS+ scheme at conditions resembling those encountered in flows around high-lift devices. Departing from the previous case with $\alpha = 16°$, $M_\infty = 0.001$, the Mach number is increased to $M_\infty = 0.1$ and $M_\infty = 0.2$. Due to the strong acceleration around the leading edge of the airfoil, regions of compressible flow will be embedded in the nearly incompressible oncoming flow. For $M_\infty = 0.2$, the highest local Mach number in the leading edge region was observed to be $M = 1.3$, and Fig. 9 gives a view of the corresponding Mach

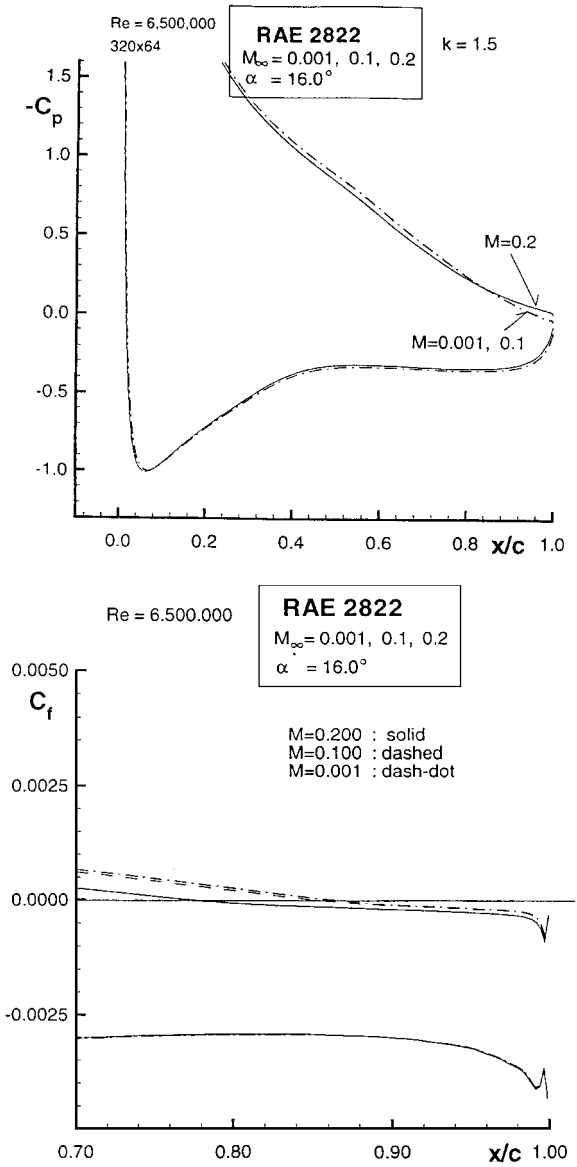

FIG. 11. Pressure and skin friction distributions for high-lift airfoil flow.

number distribution in the flow field. Figure 10 displays the corresponding convergence rates. The number of iterations at a high residual level increases with increasing Mach number. The asymptotic convergence rates are, however, almost identical. All computations were started from freestream conditions and $k = 1.5$. The reason for the increasing number of iterations may again be found by inspection of pressure distributions and corresponding skin friction distributions (Fig. 11): Increasing the Mach number increases the separation region at the trailing edge, and it is assumed that the larger the separation region, the longer the solution needs to settle to a steady condition. Once this is established, the asymptotic convergence is found to be independent of the Mach number.

5. CONCLUSION

A hybrid flux-splitting scheme was derived for solution of compressible and incompressible Euler and Navier–Stokes equations. As a basis for the derivation, a recently developed hybrid flux-splitting scheme for compressible flow was used.

Applying preconditioning techniques to solve for incompressible flows with the basic scheme, it was realized that the scheme, as other common hybrid flux-splitting schemes, does not provide any acoustic damping in the crossflow direction. To identify terms important at low Mach number flows, the well-known flux difference splitting of Roe was expanded in functions of the cell interface Mach number. In the resulting expressions, the physical relevance of the different terms occurring became obvious, and terms contributing to crossflow diffusion could clearly be identified. These findings were confirmed by numerical experiment.

The crossflow diffusion terms were then incorporated into the basic flux-splitting scheme. The resulting discretization now shows a close resemblance to the Roe flux-difference splitting; however, the weighting of several terms with the Mach number is different. The augmented flux-splitting scheme shows no degradations for compressible flows compared to the basic scheme. Using the augmented scheme in combination with preconditioning, for airfoil flows similar convergence rates could be established for incompressible and transonic flows. The robustness of the present formulation in combination with preconditioning was demonstrated by computing an airfoil under high-lift conditions with mixed incompressible and compressible flow.

ACKNOWLEDGMENTS

The author is grateful to Dr. Rolf Radespiel, DLR, for providing the hypersonic node-centered code and for his contributions to solving the hypersonic test problem. Parts of this study were conducted when the author was in residence at the Institute for Computer Applications in Science and Engineering, ICASE, and the author expresses his thanks to Dr. Manuel Salas, ICASE Director, for providing this opportunity. Special thanks go to the reviewers for their helpful comments to improve the manuscript.

REFERENCES

1. P. L. Roe, Approximate Riemann solvers, parameter vectors and difference schemes, *J. Comput. Phys.* **43**, 357 (1981).
2. B. Van Leer, Flux vector splitting for the Euler equations, in *Proceedings of 8th Int. Conference on Methodology for Hyperbolic Conservation Laws* (Springer–Verlag, Berlin, 1982).
3. M.-S. Liou and C. J. Steffen, A new flux splitting scheme, *J. Comput. Phys.* **107**, 23 (1993).
4. J. R. Edwards, A low-diffusion flux-splitting scheme for Navier–Stokes calculations, *Comp. Fluids*, **26**(6), 653 (1997).
5. A. Jameson, Artificial Diffusion, Upwind Biasing, Limiters and their Effect on Accuracy and Multigrid Convergence in Transonic and Hypersonic Flow (unpublished), AIAA Paper 93-3559 (1993).
6. R. C. Swanson, R. Radespiel, and E. Turkel, On some numerical dissipation schemes, *J. Comput. Phys.* **147**, 518 (1998).
7. C.-C. Rossow, A Simple Flux-Vector Splitting Scheme for Compressible Flows, Contributions to the 11th STAB/DGLR Symposium Berlin 1998, *in* Notes on Numerical Fluid Mechanics, Vol. 72, Vieweg Publishers, Braunschweig/Wiesbaden (1999).
8. Y.-H. Choi and C. L. Merkle, The application of preconditioning to viscous flows, *J. Comput. Phys.* **105**, 207 (1993).

9. J. M. Weiss and W. A. Smith, Preconditioning Applied to Variable and Constant Density Time-Accurate Flows on Unstructured Meshes (unpublished), AIAA Paper 94-2209 (1994).
10. R. Radespiel, E. Turkel, and N. Kroll, Assessment of Preconditioning Methods, DLR-Forschungsbericht FB 95-29 (1995).
11. B. S. Baldwin and H. Lomax, Thin Layer Approximation and Algebraic Turbulence Model for Separated Turbulent Flows (unpublished), AIAA paper 78-257 (1978).
12. R. Radespiel, C.-C. Rossow, and R. C. Swanson, An efficient cell-vertex multigrid scheme for the three-dimensional Navier–Stokes equations, *AIAA J.* **28**(8), 1464 (1990).
13. P. L. Roe and J. Pike, Efficient construction and utilization of approximate Riemann solutions, in *Computing Methods in Applied Science and Engineering* (North Holland, 1984).
14. J. R. Edwards and M.-S. Liou, Low-diffusion flux-splitting methods for flows at all speeds, *AIAA J.* **36**, 1610 (1997).
15. P. H. Cook, M. A. McDonald, and M. C. P. Firmin, Aerofoil RAE2822 Pressure Distributions and Boundary Layer and Wake Measurements, AGARD-AR-138 (1979).